Light-Activated generation of nitric oxide (NO) and sulfite anion radicals (SO3-) from a ruthenium(ii) nitrosylsulphito complex

Antonio C. Roveda Jr., Willy G. Santos, Maykon L. Souza, Charles N. Adelson, Felipe S. Gonçalves, Eduardo E. Castellano, Claudio Garino, Douglas W. Franco, Daniel R. Cardoso.

Light-activated generation of nitric oxide (NO) and sulfite anion radicals ($SO_3^{\bullet -}$) from a ruthenium(II) nitrosylsulphito complex.

Dalton Transactions, 48, 2019, 10812-10823.

DOI: 10.1039/c9dt01432b

Light-activated generation of nitric oxide (NO) and sulfite anion radicals ($SO_3^{\bullet-}$) from a ruthenium(II) nitrosylsulphito complex†

A.C. Roveda Jr.*[a], W.G. Santos[a], M.L. Souza[a], C.N. Adelson[b], F.S. Gonçalves[a], E.E. Castellano[c], C. Garino[d], D.W. Franco[a], D.R. Cardoso*[a]

[a]São Carlos Institute of Chemistry, University of São Paulo, CEP 13560-970, São Carlos, SP, Brazil. E-mail: *acroveda@usp.br*, *drcardoso@usp.br*
[b] Dept. of Chemistry, Stanford University, CA, USA
[c]São Carlos Institute of Physics, University of São Paulo, São Carlos, SP, Brazil
[d]Dept. of Chemistry and NIS Interdepartmental Centre, University of Turin, Italy

Abstract

This manuscript describes the preparation of a new Ru(II) nitrosylsulphito complex, trans-$[Ru(NH_3)_4(isn)(N(O)SO_3)]^+$ (complex **1**), its spectroscopic and structural characterization, photochemistry, and thermal reactivity. Complex **1** was obtained by the reaction of sulfite ions (SO_3^{2-}) with the nitrosyl complex trans-$[Ru(NH_3)_4(isn)(NO)]^{3+}$ (complex **2**) in aqueous solution resulting in the formation of the N-bonded nitrosylsulphito ($N(O)SO_3$) ligand. To the best of our knowledge, only four nitrosylsulphito metal complexes have been described so far (J. Chem. Soc., Dalton Trans., 1983, 2465–2472), and there is no information about the photochemistry of such complexes. Complex **1** was characterized by spectroscopic means (UV-Vis, EPR, FT-IR, ^{1}H- and ^{15}N-NMR), elemental analysis and single-crystal X-ray diffraction. The X-ray structure of the precursor complex **2** is also discussed in the manuscript and is used as a reference for comparisons with the structure of **1**. Complex **1** is water-soluble and kinetically stable at pH 7.4, with a first-order rate constant of 3.1×10^{-5} s^{-1} for isn labilization at 298 K ($t_{1/2} \sim 373$ min). Under acidic conditions (1.0 M trifluoroacetic acid), **1** is stoichiometrically converted into the precursor complex **2**. The reaction of hydroxide ions (OH^-) with **1** and with **2** yields the Ru(II) nitro complex trans-$[Ru(NH_3)_4(isn)(NO_2)]^+$ with second-order rate constants of 2.1 and 10.5 $M^{-1}s^{-1}$ (at 288 K), respectively, showing the nucleophilic attack of OH^- at the nitrosyl in **2** (Ru–NO) and at the nitrosylsulphito in **1** (Ru–$N(O)SO_3$). The pKa value of the $-SO_3$ moiety of the $N(O)SO_3$ ligand in **1** was determined to be 5.08 ± 0.06 (at 298 K).

The unprecedented photochemistry of a nitrosylsulphito complex is investigated in detail with **1**. The proposed mechanism is based on experimental (UV-Vis, EPR, NMR and Transient Absorption Laser Flash Photolysis) and theoretical data (DFT) and involves photorelease of the $N(O)SO_3^-$ ligand followed by formation of nitric oxide ($NO^\bullet$) and sulfite radicals ($SO_3^{\bullet-}$, sulfur trioxide anion radical).

†This paper is dedicated in memoriam of Prof. Dr Douglas Wagner Franco.

1. Introduction

Although the sulfite ion (SO_3^{2-}) is potentially toxic to living cells, this species is widely applied as an antioxidant and preservative in food and beverages [2], and its chemistry has received increasing attention in the last few years [2b,3]. The SO_3^{2-} anion influences the metabolism of thiocyanate (SCN^-) and nitrite (NO_2^-) in the human saliva and stomach [2a], and has been associated with several physiological conditions, such as the enhancement and suppression of nitrite-dependent $NO^\bullet$ production in the stomach [2a], skin and respiratory tract health, and anaphylactic reactions [2b]. SO_3^{2-} is metabolized by the enzyme sulfite oxidase [3c,4], for which deficiency may be lethal to humans. Most of the SO_3^{2-} toxicity is related to the production of SO_X anion radicals, formed through chain propagation steps (eqn (1)–(4)) [3d,5]:

$$SO_3^{2-} \rightarrow SO_3^{\bullet-} + e^- \quad (1)$$

$$SO_3^{\bullet-} + O_2 \rightarrow {}^-O_3SOO^\bullet \qquad k = 1.5 \times 10^9\ M^{-1}s^{-1} \quad (2)$$

$${}^-O_3SOO^\bullet + SO_3^{2-} \rightarrow SO_4^{\bullet-} + SO_4^{2-} \qquad k = 1.3 \times 10^7\ M^{-1}s^{-1} \quad (3)$$

$$SO_4^{\bullet-} + SO_3^{2-} \rightarrow SO_4^{2-} + SO_3^{\bullet-} \qquad k > 2 \times 10^9\ M^{-1}s^{-1} \quad (4)$$

Oxidation of SO_3^{2-} yields the sulfite anion radical ($SO_3^{\bullet-}$), eqn (1), which in the presence of O_2 reacts to form the oxygen-centered radicals, peroxymonosulfate radical anion ($SO_5^{\bullet-}$) and sulfate radical anion ($SO_4^{\bullet-}$), eqn (2)–(4). Recent studies showed that $SO_3^{\bullet-}$ could be produced through oxidation of SO_3^{2-} by prostaglandin H synthase, myeloperoxidase, human eosinophil peroxidase and cytochromec. 3b–f $SO_3^{\bullet-}$ and $SO_5^{\bullet-}$ are mild oxidants (E° = 0.63 V and 1.1 V vs. NHE at pH 7, respectively) [5b,6], but are precursors of the sulfate radical anion ($SO4^{\bullet-}$) (eqn(1)–(4)), a strong oxidant (E°=2.5–3.1 V vs. NHE) [5b,7] comparable to the hydroxyl radical [8]. Due to its oxidizing strength, $SO_4^{\bullet-}$ has been widely studied and recently applied in advanced oxidation process technologies [9], DNA damage [10] and organic synthesis [11].

Analogously to SO_3^{2-}, the NO^{2-} ion is also used as an antioxidant and preservative in food and beverages [2a], and the reaction between these ions is argued to produce the somewhat elusive nitrososulfonate ion ($O{\equiv}N{-}SO_3^-$, described from herein as $N(O)SO_3^-$) in the human stomach [2a]. $N(O)SO_3^-$ is considered an intermediate of several nitrogen reactive species [2a,12], such as nitric oxide ($NO^\bullet$), hydroxyimidogen (NOH) and hyponitrous acid ($H_2N_2O_2$). Furthermore, the $N(O)SO_3^-$ ion has also been proposed as an intermediate in the Raschig synthesis of hydroxylamine [1,12,13]. Nevertheless, little is known about the chemistry and physical properties of $N(O)SO_3^-$. The only compounds isolated and characterized are the N-bonded derivative species generated by the Boedeker Reaction, i.e. the nitrosylsulphito complexes $[Fe(CN)_5N(O)SO_3]^{4-}$ [13,14], $[RuCl(py)_4N(O)SO_3]$ (py = pyridine) and *cis*-$[RuX(bipy)_2N(O)SO_3]$ (X = Cl^- or Br^-, bipy = 2,2′-bipyridine) [1], of which, only the structure of *cis*-$[RuCl(bipy)_2N(O)SO_3]$ has been crystallographically characterized [1]. The reactivity of these complexes has not yet been fully studied mainly owing to their insolubility and instability [1]. Moreover, the photochemistry of the $N(O)SO_3^-$ ion and the related nitrosylsulphito complexes has never been described.

Herein we describe the reactivity of $N(O)SO_3^-$ coordinated to a Ru(II) complex, *trans*-$[Ru(NH_3)_4(isn)(N(O)SO_3)]^+$ (complex **1**, isn = isonicotinamide), Fig. 1. This complex was synthesized by the reaction of the Ru(II) nitrosyl complex *trans*-$[Ru(NH_3)_4(isn)(NO)]^{3+}$ (complex **2** in Fig. 1) with SO_3^{2-}, eqn (5):

$$\textit{trans}\text{-}[Ru(NH_3)_4(isn)(NO)]^{3+} + SO_3^{2-} \rightarrow \textit{trans}\text{-}[Ru(NH_3)_4(isn)(N(O)SO_3)]^+ \quad (5)$$

The family of *trans*-$[Ru(NH_3)_4(L)(NO)]^{3+}$ complexes is well known to be kinetically stable and water-soluble [15], supporting the choice of this type of nitrosyl as the synthetic precursor of complex **1**. As expected, **1** is water-soluble and kinetically stable at pH 7.4 (at 298 K), and the $N(O)SO_3^-$ ion is stabilized upon coordination to Ru(II), making studying its reactivity possible. The solubility and stability of **1** in water are higher than those of all four previously reported complexes $[L_5M–N(O)SO_3]^n$ (M = Fe, Ru). Our investigations on **1** also contribute to a current interesting topic in the chemistry of nitrosyl complexes and sulfur nucleophiles [16], and of S, N, O species [16c,17]. Moreover, the light-triggered generation of the relevant radicals ($NO^{\bullet}$ and $SO_3^{\bullet-}$) from **1** may find utility in many important redox and photochemical based applications [18].

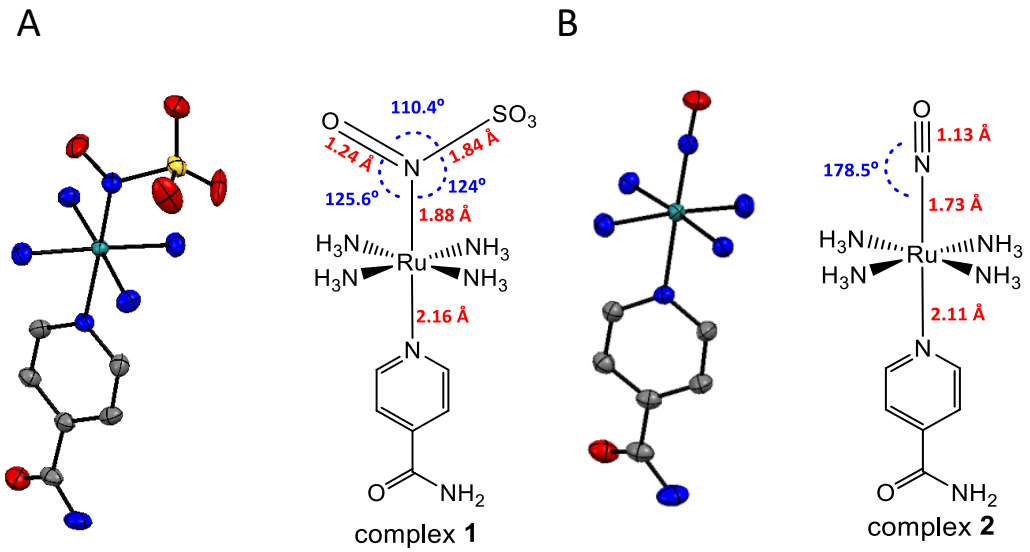

Fig. 1. X-ray and molecular structures of complexes (A) **1** and (B) **2**. The numbers in red show the bond lengths, and in blue, the angles. Ellipsoids at 50% probability; H omitted for clarity.

2. Results and discussion

2.1. X-ray crystallography and Infrared spectroscopy

The reaction of the nitrosyl complex *trans*-$[Ru(NH_3)_4(isn)(NO)]^{3+}$ (**2**) with SO_3^{2-} (eqn (5)) yields the new nitrosylsulphitoion complex *trans*-$[Ru(NH_3)_4(isn)(N(O)SO_3)]_+$ (**1**), Fig. 1, a green solid. This reaction occurs through the nucleophilic addition of the sulfite ion to the nitrogen atom of the nitrosyl moiety (Ru–NO) of complex **2**. Complex **1** was characterized by elemental analysis and by several spectroscopies, and the experimental data correlated well with the DFT calculations (see the ESI).

The crystal structures of **1** and of its synthetic precursor (**2**) are shown in Fig. 1. Table 1 shows the main bond lengths and angles for **1**, **2** and for a previously described nitrosylsulphito complex, *cis*-$[RuCl(bipy)_2N(O)SO_3]$ (**3**) [1].

Table 1. Selected bond lengths and angles for the complexes *trans*-$[Ru(NH_3)_4(isn)(N(O)SO_3)]^+$ (**1**), *trans*-$[Ru(NH_3)_4(isn)(NO)]^{3+}$ (**2**) and *cis*-$[RuCl(bipy)_2N(O)SO_3]$ (**3**).

	Ru Complex		
	1 [a]	**2** [a]	**3** [b]
Distances (Å)			
Ru–N ($\underline{N}(O)SO_3$ or $\underline{N}O$)	1.877(3)	1.750(3)	1.904(14)
N–O	1.244(5)	1.119(4)	1.208(17)
N–S	1.844(4)	—	1.820(15)
Ru–N_{isn}	2.167(3)	2.099(3)	—
Ru–NH_3 [c]	2.12	2.10	—
Angles (°)			
Ru–N–O	124.4(4)	175.4(3)	123.8(12)
Ru–N–S	124.2(19)	—	127.9(7)
O–N–S	110.4(3)	—	108.0(11)
N_{isn}–Ru–N ($\underline{N}(O)SO_3$ or $\underline{N}O$)	178.32(14)	177.39(12)	—

[a]This Work. [b]Ref. 1. [c]Average of the four Ru–NH_3 bonds.

In both complexes **1** and **2** (Fig. 1), the aromatic moiety of the isn ligand is perpendicular to the plane formed by the four nitrogens of the equatorial ammines (NH_3) and bisects two opposite N–Ru–N angles of NH_3. The N_{isn}–Ru–$N_{N(O)SO3}$ bond angle in **1** is almost linear and very close to that observed for the N_{isn}–Ru–N_{NO} bond angle in **2** (Table 1). Complexes **1** and **2** have slightly different Ru–NH_3 bond distances (Table 1). The Ru–$N(O)SO_3$ bond length in **1** is ~0.24 Å shorter than the average of the four Ru–NH_3 distances (Table 1), showing an increase in the bond order in Ru–$N(O)SO_3$ relative to Ru–NH_3 due to π interactions in the former. A similar behavior is observed for complex **2**. However, the Ru–NO bond length in **2** is ~0.13 Å shorter than the Ru–$N(O)SO_3$ bond length in **1** (Fig. 1 and Table 1). This indicates a stronger back-bonding of the NO ligand in **2** than that of the $N(O)SO_3$ ligand in **1**. This result is consistent with the Ru–N–O angle, which is close to linear in **2** (175.4°) and is 124.4° in **1** (Fig. 1). The linear angle of Ru–N–O provides a greater overlap of the Ru dπ orbital with the π* orbital of NO in **2** [19], and consequently, a stronger Ru–NO bond in **2** than the Ru–$N(O)SO_3$ bond in **1**.

The longer Ru–N_{isn} bond length in **1** than in **2** (Fig. 1 and Table 1) shows a stronger trans-influence of the $N(O)SO_3$ ligand than that of the NO ligand, regarding isn in the trans position. Furthermore, the S–N bond length of ~1.84 Å for the $N(O)SO_3$ ligand in **1** is ca. 10% longer than that of other S–N compounds, e.g. nitrosopersulfide ($SSNO^-$) and thionitrite (SNO^-), 1.689 Å and 1.707 Å, respectively [16c]. It is also longer than S-nitrosothiols coordinated to transition metal complexes [16g,h].

The Ru–N–O and Ru–N–S angles in **1** (124.4° and 125.2°, respectively) are slightly different from those reported for a closely related complex, *trans*-$[Ru(NH_3)_4P(OEt)_3(NO_2)](PF_6)$, in which the Ru–N–O angle is 120.9° for one of the oxygen atoms of the NO_2 ligand, and 121.4° for the other [20] The Ru–N–O, Ru–N–S and O–N–S angles in **1** are close to those reported for S-nitrosothiols coordinated to transition metal complexes [16g,h]. For the $N(O)SO_3$ ligand in **1**, the S–O bond lengths are shorter than those in sodium sulfite (Na_2SO_3), ~1.40 Å and 1.53 Å, respectively. However, the O–S–O angles are larger in **1** than those in Na_2SO_3, 112–117° and 107.4°, respectively [21].

The bond lengths and angles for the [RuN(O)SO_3] moiety of complex **1** are very similar to those reported for *cis*-[RuCl(bipy)$_2$(N(O)SO_3)] (complex **3**) [1], with differences lower than 0.04 Å and 3° for the bond lengths and angles, respectively, Table 1. Therefore, despite considerable differences in the coordination spheres of **1** and **3**, there were no significant discrepancies among the bond angles and bond distances of the [Ru–N(O)SO_3] fragments in these complexes.

The FT-IR spectra of **1** and **2** are shown in Fig. S1 (ESI) and the main IR frequencies of the complexes **1**, **2**, $[Fe(CN)_5N(O)SO_3]^{4-}$, [RuCl(py)$_4$N(O)SO_3] and *cis*-[RuX(bipy)$_2$N(O)SO_3] (X = Cl^- or Br^-) [13,14] are shown in Table 2. The ν(NO) observed for **2** at 1933 cm^{-1} was shifted to 1366 cm^{-1} on **1** (Table 2, and Fig. S1 ESI). This shift is consistent with the weakening of the N–O bond in **1** (1.24 Å) in comparison with **2** (1.12 Å) (Fig. 1 and Table 1). All the IR bands observed for the nitrosylsulphito complexes showed similar frequencies for the N(O)SO_3 moiety, with differences lower than 30 cm^{-1} (Table 2). These data revealed that the vibrational frequencies of the N(O)SO_3 moiety were not strongly affected by modifications in the coordination sphere of the complexes, in agreement with the X-ray results as discussed above for **1** and **3**.

Table 2. Main Vibrational bands (cm^{-1}) and assignments for a series of $[L_5M–(N(O)SO_3)]^n$ complexes [1], and for complex **2**.

Complex	Assignment[c]					
	ν(N–O)	ν_{asym} (S–O)	ν_{sym} (S–O)	ν_{sim} (S–O)	δ_{asym} (O–N–S)	δ_{asym} (O–S–O)
$Cs_4[Fe(CN)_5(N(O)SO_3)]$[a]	1357s	1252s	1229s	1041s	758w	621s
trans-[RuCl(py)$_4$(N(O)SO_3)][a]	1346s	1273sh	1258s	1031s	770	604
cis-[RuBr(bipy)$_2$(N(O)SO_3)] [a]	1372s	1270sh	1255s	1040s	775	605s
cis-[RuCl(bipy)$_2$(N(O)SO_3)] (**3**) [a]	1370s	1267sh	1250s	1038s	775	612
trans-$[Ru(NH_3)_4(isn)(N(O)SO_3)]^+$ (**1**) [b]	1366s	1263sh	1225s	1040s	778m	623s
trans-$[Ru(NH_3)_4(isn)(NO)]^{3+}$ (**2**) [b]	1933s	—	—	—	—	—

[a]ref. 1; [b]this work; s = strong; m = medium; w = weak; sh = shoulder

2.2 Electronic structure, ^{1}H- and ^{15}N-NMR, and EPR spectroscopy

Complex **1** has two doublets in the ^{1}H-NMR spectrum with chemical shifts (δ) at δ = 8.87 and 8.13 ppm (Fig. S2, ESI), assigned respectively to the *ortho* and *meta* hydrogens of the isn ligand in **1**. The ^{15}N-NMR spectrum of **1** only exhibits one peak at δ = 192.8 ppm (Fig. S3, ESI). The sharp narrow-width peaks observed in the ^{1}H-NMR spectrum and the lack of EPR signals (EPR silent at 77 K) are consistent with a S = 0 ground state of **1**, in agreement with the electronic structure description for the parent precursor nitrosyl complex **2**, and for the family of *trans*-$[Ru(NH_3)_4(L)(NO)]^{3+}$ complexes [15,22].

Nucleophilic attack at coordinated nitrosyls in ruthenium and iron complexes is well documented in the literature [16a,23]. In the case of the family of *trans*-$[Ru(NH_3)_4(L)(NO)]^{3+}$ complexes, nucleophilic attack of OH^- or of thiols occurs on the nitrosyl ligand (Ru–NO) and leads to species with an intense and broad band in the long-wave UV and visible ranges of the spectra [16a,f,i,24]. This behavior is consistent with the electronic absorption band observed for **1** at λ_{max} = 363 nm (Fig. 2) formed after the nucleophilic addition of SO_3^{2-} to the nitrosyl ligand of **2** (eqn (5)). This intense band ($\varepsilon = 6.0\times10^3$ $M^{-1}cm^{-1}$) was assigned by TD-DFT as a metal to ligand charge transfer

(MLCT) transition, Ru → $N(O)SO_3$ (inset of Fig. 2B; Fig. S6, S7, Table S5, ESI). This MLCT transition is of higher energy in comparison with that of the complexes $[Fe(CN)_5N(O)SO_3]^{4-}$, $[RuCl(py)_4N(O)SO_3]$ and cis-$[RuX(bipy)_2N(O)SO_3]$ (X = Cl^- or Br^-) [1], which are in the range of 450–475 nm [1]. The theoretical spectrum of **1** is in agreement with the experimental results (Fig. 2B and S6 of the ESI), and the detailed assignments of all the electronic absorption bands of **1** are given in Table S5 (ESI).

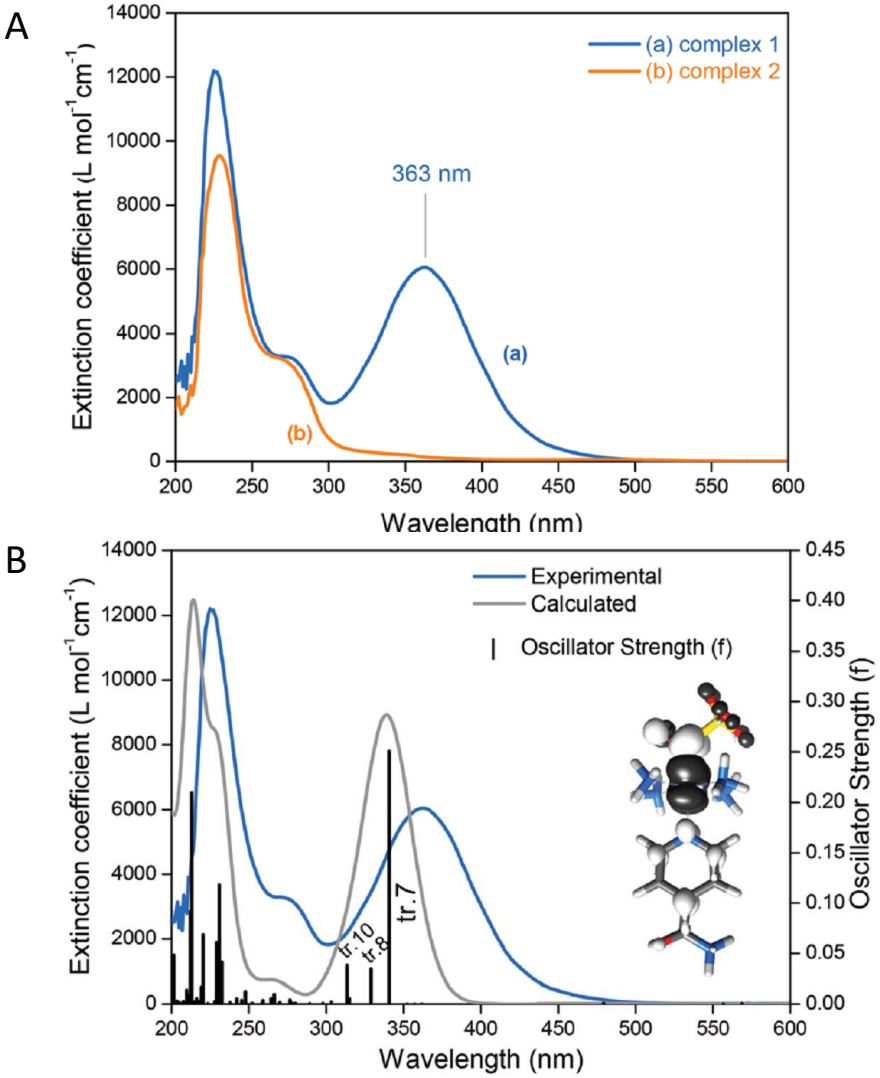

Fig. 2. Electronic absorption spectra (UV-Vis) of the complexes **1** and **2**, both in phosphate buffer pH 7.4. (B) Experimental and theoretical UV-Vis of **1**. Electronic transitions are represented as vertical bars with height equal to the oscillator strength (f) values. tr. 7, 8 and 10 = electronic transitions #7, #8 and #10, respectively. Inset: Electron-density difference maps (EDDM) of the tr. 7, a MLCT Ru → $N(O)SO_3$ (black indicates a decrease in electron density, white indicates an increase; isovalue = 0.001).

2.3 Thermal stability of 1 at pH 7.4 and under acidic conditions

The thermal stability of **1** was investigated using electronic absorption (UV-Vis) and ^{1}H-NMR spectroscopy (Fig. S8–S11, ESI), and the results showed that **1** is kinetically stable at pH 7.4, with a rate constant of 3.1×10^{-5} s^{-1} for isn labilization at 298 K ($t_{1/2}$ ~ 373 min). The activation parameters for the isn labilization from **1** are listed in Table S6 (ESI). This reaction is governed by the positive

values of the enthalpic ($\Delta H \approx 26.5$ kcal mol^{-1}) and entropic terms ($\Delta S \approx 9.1$ cal $mol^{-1}K^{-1}$), suggesting a dissociative (I_d) rate-determining step. The product formed after isn labilization from **1** was characterized by ^{15}N-NMR (using ^{15}N-labeled $N(O)SO_3$ ligand in **1**) as being the hydroxo nitrosyl complex [25] *trans*-$[Ru(NH_3)_4(OH)(^{15}NO)]^{2+}$, at $\delta \sim -40.3$ ppm [25] (Fig. S12 and S13, ESI). Correspondingly, the decomposition of *trans*-$[RuCl(py)_4N(O)SO_3]$ in neutral solution also yields the hydroxo nitrosyl complex $[RuOH(py)_4NO]^{2+}$ [1].

In acidic solution (1.0 M trifluoroacetic acid), complex **1** was stoichiometrically converted into the precursor nitrosyl (complex **2**) by heterolytic cleavage of the S–N bond of the $N(O)SO_3$ moiety, based on the FT-IR and ^1H-NMR results (Fig. S14 and S15 ESI). These findings are in agreement with the data reported for the complexes *cis*-$[RuCl(bipy)_2(N(O)SO_3]$ and *trans*-$[RuCl(py)_4(N(O)SO_3)]$ in aqueous HCl (4.0 M) [1].

2.4 The reaction of hydroxide ions (OH−) with the complexes 1 and 2

One of the main topics of interest in nitrosyl chemistry is metal nitrosyl complex electrophilicity [1,16a,23,24,26]. The reaction of nitrosyl complexes with a variety of nucleophiles is well documented, and the main species studied are OH^-,HS^-,N_3^-, NH_2OH and RS^- (thiols). Aiming to investigate the electrophilic character of the $N(O)SO_3$ ligand in **1**, the reaction of this complex and also that of complex **2** with OH^- were performed. Of note, in general, nitrosyl complexes of the type $[L_5M(NO)]^n$ react with OH^- yielding the respective nitro complexes $[L_5M(NO_2)]^{(n-2)}$ [16a,24]. This reaction was already investigated for a series of *trans*-$[Ru(NH_3)_4(L)(NO)]^{3+}$ nitrosyl complexes [24], but here we show unprecedented electrophilic behavior of a nitrosylsulphito complex.

Both the reactions of **1** and **2** with OH^- produced the respective nitro complex *trans*-$[Ru(NH_3)_4(isn)(NO_2)]^+$ [15,24], with a characteristic band at $\lambda = 404$ nm (Fig. 3). During the reaction of **1** with OH^-, the characteristic band of **1** at 363 nm decreases at the rate that the 404 nm band grows in (Fig. 3A), with an isosbestic point at 375 nm. Analogously, the 404 nm band appears as complex **2** reacts with OH^-. These results were confirmed by ^{15}N-NMR spectroscopy, by means of comparisons of the reaction of OH^- with ^{15}N-labelled **1** and **2** (Fig. S16, ESI) [15,24]. The formation of a single peak at $\delta^{15}_N = 158.2$ ppm in the ^{15}N-NMR (Fig. S16, ESI) confirmed that the reactions of **1** and **2** with OH^- yielded the same product, i.e. the complex *trans*-$[Ru(NH_3)_4(isn)(NO_2)]^+$ [15,24].

A complete set of kinetic data for the reaction of OH^- with **1** and with **2** is provided in the ESI (Fig. S17, S18 and Table S7). Under pseudo-first-order conditions ($[OH^-] \gg$ [complexes **1** or **2**]) the rate constants for the formation of *trans*-$[Ru(NH_3)_4(isn)(NO_2)]^+$ are 2.1 and 10.5 $M^{-1}s^{-1}$ (at 288 K) for **1** and **2**, respectively (Table S7, ESI). The mechanism of the reaction of **1** with OH^- was investigated by DFT calculations, and the results showed that the formation of *trans*-$[Ru(NH_3)_4(isn)(NO_2)]^+$ occurs by the nucleophilic attack of OH^- on the nitrogen atom of the $N(O)SO_3$ ligand in **1** (Fig. S19 and Table S8, ESI). This finding is in agreement with our experimental results (UV-Vis and ^{15}N-NMR, Fig.3 and Fig. S16 (ESI), respectively) and is comparable to the mechanism reported for the reaction of OH^- with the family of *trans*-$[Ru(NH_3)_4(L)(NO)]^{3+}$ complexes [15,24].

Therefore, the experimental and DFT data showed for the first time the susceptibility of a nitrosylsulphito ligand to nucleophilic attack by hydroxide ions, then yielding the respective Ru(II) nitro complex.

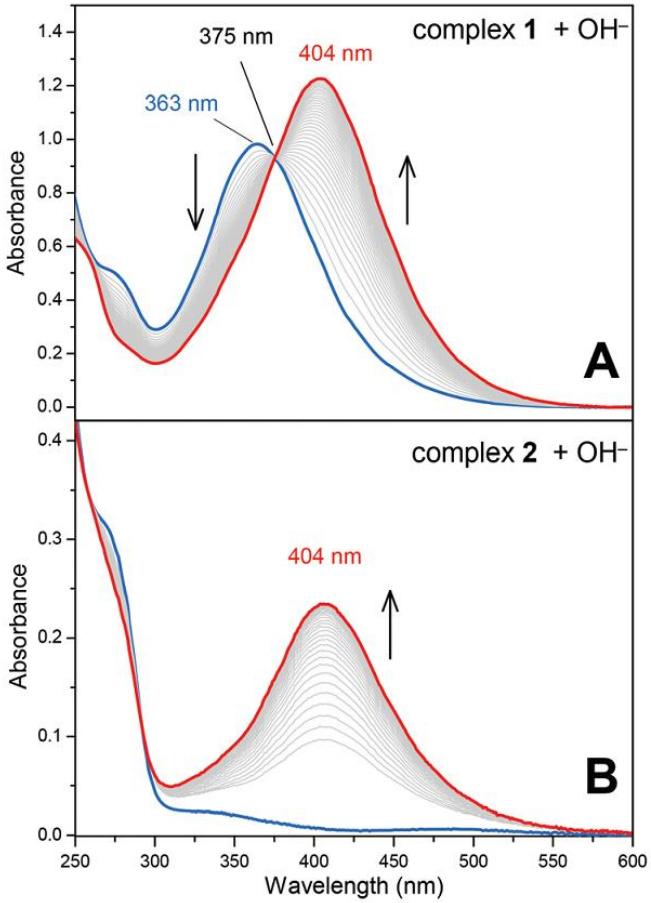

Fig. 3. Representative spectral changes for the reaction of OH^- with the complexes **1** (A) and **2** (B).

2.5 pKa of the N(O)SO₃ ligand in complex 1

The pKa of the $N(O)SO_3$ ligand was determined spectrophotometrically through titration of **1** with aqueous trifluoroacetic acid solutions (Fig. S20A, ESI). The titration curve is shown in Fig. S20B (ESI), and the pKa values obtained by two treatments (see the Experimental section; Fig. S20B and S21A, ESI) were 5.03 and 5.12, respectively, for the protonation shown in eqn (6):

$$\textit{trans}\text{-}[Ru(NH_3)_4(isn)(N(O)SO_3)]^+ + H_3O^+ \rightleftharpoons \textit{trans}\text{-}[Ru(NH_3)_4(isn)(N(O)SO_2OH)]^{2+} + H_2O \qquad (6)$$

Unfortunately, no previous studies on nitrosylsulphito complexes reported pKa values, thus making comparisons not possible. However, the pKa determined for **1** (eqn (6)) is within an expected range given that the sulfite ion (SO_3^{2-}, non-coordinated) has a pKa value of 7.2 (ref. 4c) and that this value should diminish upon coordination to the nitrosyl precursor (eqn (5)). From these values, we can estimate that the pKa of the free $N(O)SO_3^-$ ion (non-coordinated to the Ru complex) is between $5.1 < pKa < 7.2$ (for the protonation of one of the oxygen atoms of the SO_3 moiety).

2.6 Photochemistry

Irradiation of **1** with light of wavelengths of 355 or 410 nm produces $NO^{\bullet}$, $SO_3^{\bullet-}$ and isn in solution, and no Ru(III), as discussed in detail below. Of note, since there are no available data on the photochemistry of nitrosylsulphito complexes (to the best of our knowledge) some comparisons about the photochemistry of **1** will be performed with analogous Ru(II) nitro complexes, $[L_5Ru–NO_2]^n$.

The MLCT (Ru → N(O)SO_3) band at 363 nm (Fig. 2A) decreases with the irradiation time of **1** (Fig. S22, ESI), and this behavior can be associated with labilization of the N(O)SO_3^- ligand. This hypothesis corroborates the results reported for the parent nitro complex *trans*-$[Ru(NH_3)_4P(OEt)_3(NO_2)]^+$ ($P(OEt)_3$ = triethyl phosphite) [20], and also for other $[L_5Ru\text{-}NO_2]^n$ complexes [20,27], which upon irradiation the MLCT band (Ru → NO_2) decreases, resulting in labilization of NO_2^- (eqn (7)) and no Ru(III) formation:

$$[L_5Ru - NO_2]^n \xrightarrow[H_2O]{h\nu} [L_5Ru - (H_2O)]^{n+} + NO_2^- \qquad (7)$$

In some of these nitro complexes, nitric oxide ($NO^\bullet$) was also detected in solution during photolysis, and this process was related to secondary photochemical reactions [20,27b], eqn (8):

$$NO_2^- \xrightarrow[H_2O]{h\nu} NO^\bullet + O^{\bullet-} \qquad (8)$$

In analogy to eqn (7) and (8), the products most likely formed upon N(O)SO_3^- release during irradiation of **1** are the radical species $NO^\bullet$ and $SO_3^{\bullet-}$. To investigate this hypothesis, catalase was used for the detection of $NO^\bullet$, and DMPO (5,5-dimethyl-1-pyrroline-N-oxide) for the detection of $SO_3^{\bullet-}$. Of note, two well-documented procedures used for $NO^\bullet$ detection (oxymyoglobin and PTIO) [28] were not effective for distinguishing among the formation of $NO^\bullet$ or $SO_3^{\bullet-}$ (Fig. S23, S24, ESI). When **1** was irradiated in the presence of catalase two new bands appeared at 538 and 575 nm (Fig. 4A). This is in agreement with the spectral changes reported for the binding of $NO^\bullet$ to catalase [29], thus confirming the formation of $NO^\bullet$ during irradiation of **1**. The EPR results for irradiation of **1** in the presence of DMPO are depicted in Fig. 4B. The simulated spectrum and the hyperfine coupling constants (shown in the caption of Fig. 4) are consistent with those reported for the DMPO/$^\bullet SO_3^-$ adduct [3d,30], thus confirming $SO_3^{\bullet-}$ as a photoproduct of **1** (Fig. 4B). Therefore, the hypothesis that irradiation of **1** could result in the formation of $NO^\bullet$ and $SO_3^{\bullet-}$ species was confirmed.

Transient absorption Laser Flash Photolysis (LFP) studies were performed to gain further insight into the photochemistry of **1**. The transient spectra obtained after laser excitation of **1** are shown in Fig. 5A. The transient spectrum has a maximum at 480 nm (Fig. 5A), and as can be seen in Fig. 5B, this band matches the band of the aquo complex *trans*-$[Ru(NH_3)_4(H_2O)(isn)]^{2+}$ at λ_{max} = 480 nm (ref. 31) (in this aquo complex the coordinated H_2O has a pKa value of 11.7 [31a]). Therefore, the transient spectrum (Fig. 5) can be assigned to the photoproduct aquo complex trans-$[Ru(NH_3)_4(H_2O)(isn)]^{2+}$, formed upon irradiation of **1**.

LFP thus supports the hypothesis that the N(O)SO_3 ligand dissociates from the Ru center upon irradiation of **1**, forming the aquo complex and the radical species $NO^\bullet$ and $SO_3^{\bullet-}$, as summarized in Fig. 6. This mechanism is also supported by DFT calculations on the electronic excited state resulting from excitation of the MLCT Ru → N(O)SO_3 of **1** (tr. 7 in Fig. 2B).

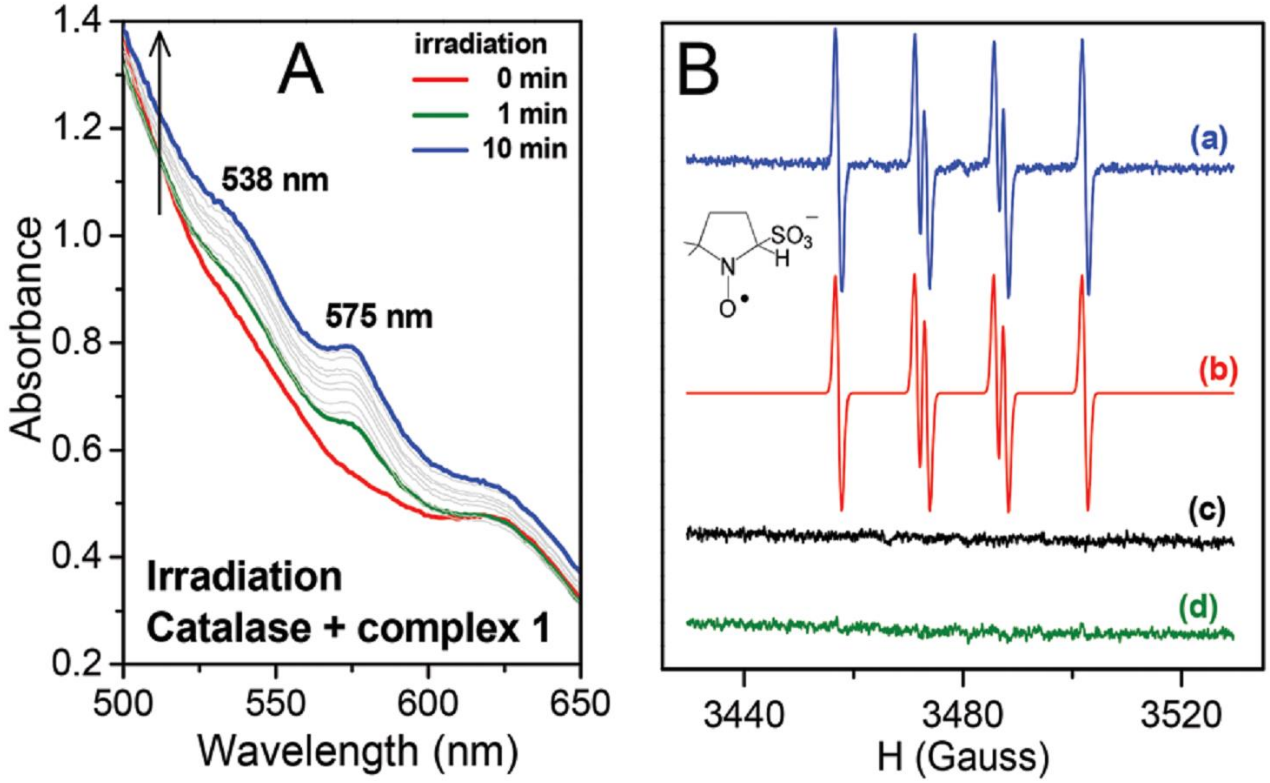

Fig. 4. Formation of $NO^{\bullet}$ and $SO_3^{\bullet-}$ during irradiation of **1**. (A) Detection of $NO^{\bullet}$ by UV-Vis: complex **1** (9.0 mM) + Catalase (~15 μM) in phosphate buffer (PBS pH 7.4, 200 mM). (B) Detection of $SO_3^{\bullet-}$ by EPR (a) EPR: complex **1** (0.2 mM) + DMPO (100 mM) irradiated for 1 min (PBS pH 7.4); (b) simulated spectrum: DMPO/$^{\bullet}SO_3^-$ radical adduct (inset), a^N = 14.45 G and a^H = 16.10 G; (c) control: PBS (pH 7.4) + DMPO (100 mM) irradiated for 5 min; (d) same solution as in (a) but before irradiation. Both (A) and (B) recorded at T = 25 °C, λ_{irrad} = 355 nm.

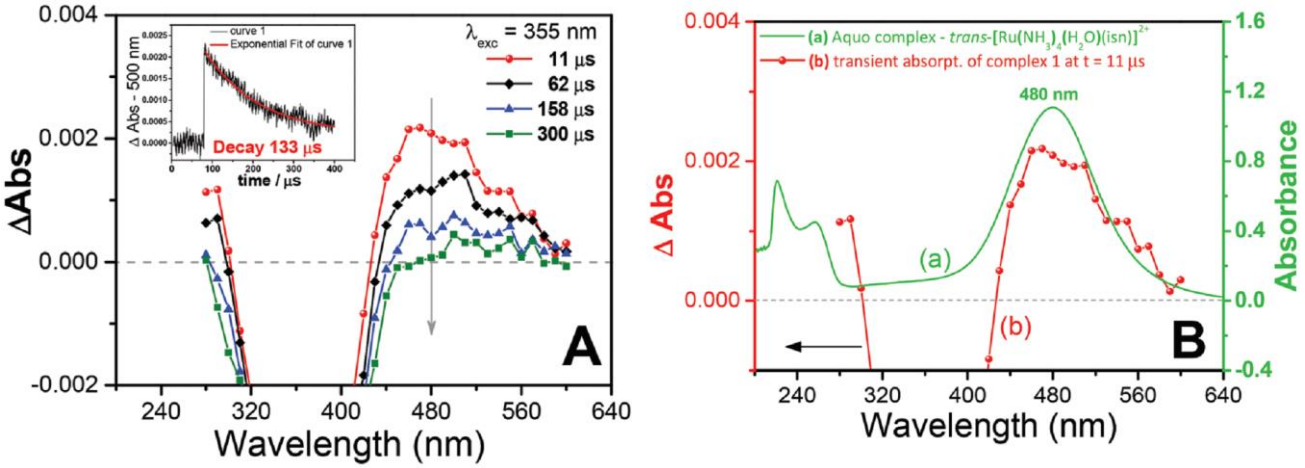

Fig. 5. Transient absorption spectra after 355 nm excitation of complex **1**. (A) Transient absorption spectra at different time intervals (11–300 μs); inset shows the decay profile at λ = 500 nm. (B) Absorption spectrum of the aquo complex *trans*-$[Ru(NH_3)_4(H_2O)(isn)]^{2+}$ and of the transient at t = 11 μs. Conditions: Phosphate buffer pH 7.4, T = 25 °C.

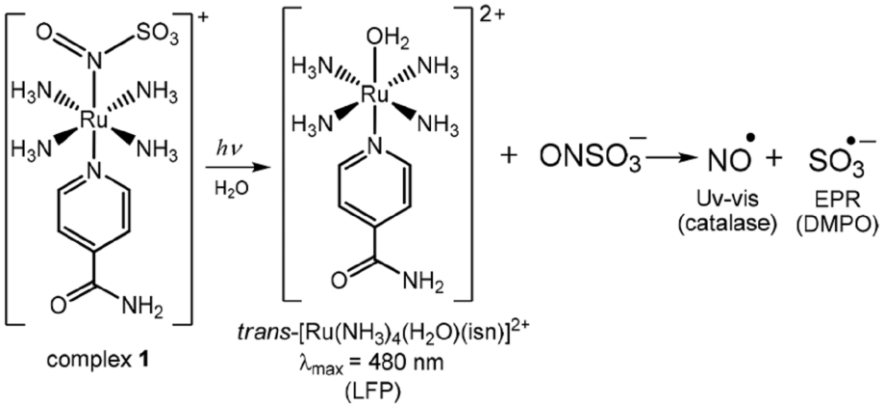

Fig. 6. Proposed photochemical mechanism of complex **1**. This mechanism is based on detection of the aquo complex *trans*-$[Ru(NH_3)_4(H_2O)(isn)]^{2+}$ by Laser Flash Photolysis (LFP), of nitric oxide (NO•) by the reaction with catalase (by Uv-Vis), of sulfite radical ($SO_3^{\bullet-}$, by EPR using DMPO as a spin trap), and on DFT results (vide infra).

The DFT analysis of the orbitals involved in this electronic transition highlights the depopulation of the bonding HOMO-2 orbital and the population of the antibonding LUMO as main components, with respect to the Ru–$N(O)SO_3$ bond (Table S5 and Fig. S7, ESI). Geometry optimization shows that the resulting electronic excited state is significantly distorted along the z-axis with respect to the GS (labeled S7 in Fig. S25, ESI), with a long Ru–$N(O)SO_3$ bond distance of 2.60 Å (for GS this bond length is calculated as ~1.91 Å), thus further supporting the mechanism of photolabilization of $N(O)SO_3^-$ from **1** (Fig. 6).

Additionally, in situ ^{1}H-NMR of the irradiation of **1** showed that the isonicotinamide ligand (isn) is also capable of photodissociating from the Ru center (Fig. S26, ESI). Since the formation of the aquo complex trans-$[Ru(NH_3)_4(H_2O)(isn)]^{2+}$ was identified by LFP (Fig. 5B), the labilization of the isn ligand thus must arise from a consecutive photochemical event, occurring after the $N(O)SO_3^-$ photolabilization, as it is most improbable that irradiation of **1** would cause simultaneous labilization of both $N(O)SO_3^-$ and isn ligands. Analogous consecutive dual photolyses have been previously reported for other Ru(II) systems, in which two ligands were photolabilized during irradiation [32]. Moreover, the band at 480 nm observed in the transient spectra (by LFP) is formed and then decays (Fig. 5A), showing that the isn labilization occurs after dissociation of $N(O)SO_3^-$ from **1**. This conclusion is based on the fact that the 480 nm band is a MLCT Ru → isn transition [31] of the aquo complex *trans*-$[Ru(NH_3)_4(H_2O)(isn)]^{2+}$, and the decay of this band would be related to the labilization of the isn ligand, in agreement with the ^{1}H-NMR results of the in situ irradiation of **1**.

Identical results to those shown in Fig. 5 were obtained when LFP experiments with complex **1** were performed in the presence of an excess of DMPO or of isonicotinamide. This result shows that the formation of the aquo complex trans-$[Ru(NH_3)_4(H_2O)(isn)]^{2+}$, followed by its decay (Fig. 5), is not directly influenced by the presence or absence of either the sulfite radical ($SO_3^{\bullet-}$) or the isn ligand in solution.

In addition, the quantum yield (ϕ) for the photoinduced labilization of the ligands in complex **1** was measured using electronic absorption spectroscopy by monitoring the decrease of its MLCT band (363 nm) during 355 nm irradiation (Fig. S22, ESI), and was calculated as $\phi = 0.12 \pm 0.03$. Very similar ϕ values were obtained by monitoring the photodissociation of isn by ^{1}H-NMR for the in situ irradiation of **1** (Fig. S26, ESI).

In summary, light irradiation of 1 leads to the labilization of $N(O)SO_3^-$, which then undergoes rapid homolysis to form $NO^\bullet$ and $SO_3^{\bullet-}$ (Fig. 6). Therefore, the two possible pathways for the formation of $NO^\bullet$ and $SO_3^{\bullet-}$ are through thermal and photochemical decomposition of the free $N(O)SO_3^-$ ion: (i) by the thermal homolysis of the S–N bond of the $N(O)SO_3^-$ ion, thus dissociating into $NO^\bullet$ and $SO_3^{\bullet-}$ radicals and (ii) by the photodecomposition of $N(O)SO_3^-$ through a process similar to that observed during photolysis of S-nitrosothiols (*via* formation of $NO^\bullet$ and thiyl radicals [33], and also analogous to the mechanism observed for the photodecomposition of the nitro ligand in Ru(II) nitro complexes [20], eqn (7) and (8)).

Molecules with S–N bonds and structures similar to $N(O)SO_3^-$, such as thionitrous acid (HSNO, S–N bond length of 1.78–1.93 Å) [34] and other S-nitrosothiols, are proposed to undergo light induced homolysis of the weak S–N bond [33]. Therefore, the two possible pathways for $N(O)SO_3^-$ decomposition, i.e. (i) thermal and (ii) photochemical S–N cleavage, are both likely to occur. The investigation of the mechanism for the formation of $NO^\bullet$ and $SO_3^{\bullet-}$ radicals from $N(O)SO_3^-$ was performed by DFT, and the results are provided in detail in the next section.

2.7 Formation of $NO^\bullet$ and $SO_3^{\bullet-}$ by the S–N bond dissociation of $N(O)SO_3^-$

As discussed in the crystallographic section, the S–N bond length of the $N(O)SO_3^-$ ligand in **1** is 1.84 Å, ca. 10% longer than that of other S–N compounds. Therefore, it is not surprising that the $N(O)SO_3^-$ anion (formed in solution after irradiation of **1**) may rapidly decompose to form $NO^\bullet$ and $SO_3^{\bullet-}$ (Fig. 6), and this event is likely to occur through thermal and photochemical reaction pathways.

Unconstrained geometry optimizations of $N(O)SO_3^-$ were performed on both the singlet and triplet surfaces. The resulting singlet structure is 10.7 kcal mol^{-1} more stable than the optimized triplet structure (thus showing that $N(O)SO_3^-$ has a singlet ground state), and has a 1.877 Å S–N bond length. The energy profile of the thermal homolysis of the S–N bond of $N(O)SO_3^-$ (singlet) is shown in Fig. 7. The transition state for homolysis has ΔG = 13 kcal mol^{-1}, a single normal mode with a low imaginary frequency of −40.85 cm^{-1} (due to the large reduced masses of the NO and SO_3 fragments, Fig. S28, ESI), and a bond length of 2.451 Å. Collectively, these geometric and electronic structure parameters indicate that the transition state is late on the homolysis pathway, and proceeds after substantial S–N bond cleavage has occurred. The $NO^\bullet$ and $SO_3^{\bullet-}$ products collectively have ΔG = 6.4 kcal mol^{-1} above that of the $N(O)SO_3^-$ molecule (Fig. 7), showing that S–N homolysis is slightly endergonic. According to the energy barrier predicted for the thermal homolysis of the S–N bond of $N(O)SO_3^-$ (ΔG = 13 kcal mol^{-1}, Fig. 7), this reaction is nearly instantaneous at room temperature (298 K). This is in agreement with the above results (Fig. 4) which demonstrated that the radicals $NO^\bullet$ and $SO_3^{\bullet-}$ are formed upon irradiation of **1**, thus corroborating with the mechanism proposed (Fig. 6).

The enthalpy of the reaction in eqn (9) at 298 K (Δ_rH_{298}), which is by definition [35] the bond dissociation enthalpy (BDE) of the ion $N(O)SO_3^-$, was calculated according to the literature [36]. The BDE of this reaction (eqn (9)) was predicted as 17.8 kcal mol^{-1}.

$$N(O)SO_3^- \rightarrow NO^\bullet + SO_3^{\bullet-} \qquad (9)$$

The S–N BDE of $N(O)SO_3^-$ is smaller than that predicted for a series of representative S-nitrosothiols (CH_3SNO, CH_3CH_2SNO, $(CH_3)_2CHSNO$, $(CH_3)_3CSNO$, CH_2CHSNO, ca. 23.3–32.4

kcal mol^{-1}) [37], and this can be explained by the fact that $SO_3^{\bullet-}$ is a resonance-stabilized radical. Indeed, this behavior was already observed in that series of S-nitrosothiols, in which the vinyl-substituted thiol (CH2CHSNO) had the smallest BDE of the series (23.3 kcal mol^{-1}) because of the resonance-stabilized thiyl radical formed after the homolytic S–N dissociation (the BDE values of the other S-nitrosothiols of the series were in the range of 31.3–32.4 kcal mol^{-1}) [37].

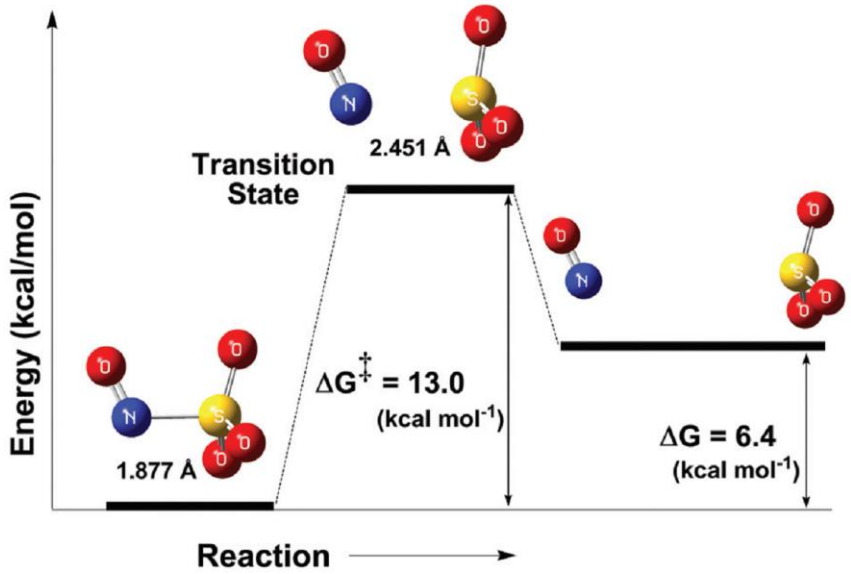

Fig. 7. Reaction coordinate of the thermal decomposition of the S–N bond of the ion $N(O)SO_3^-$ (left). Transition state (middle), and $NO^{\bullet}$ and $SO_3^{\bullet-}$ (right).

The second pathway investigated by DFT for the dissociation of the N(O)SO3– into $NO^{\bullet}$ and $SO_3^{\bullet-}$ radicals is the photochemical. The theoretical UV-Vis absorption spectrum of $N(O)SO_3^-$ is characterized by a series of transitions in the UV region, plus a transition in the far red-region (Fig. 8A). Among the seven electronic transitions (tr.1–tr.7, Fig. 8A), tr.1 and tr.2 have the smallest oscillator strengths. The first six electronic transitions (tr.1–tr.6 in Fig. 8A) all involve the population of the LUMO, that is antibonding along the S–N bond (Table S9, ESI). In particular, the first electronic excited state (S1) has strong dissociative nature. This can be clearly seen by the related electron density difference map (Fig. 8B) that shows a loss of electron density along the S–N bond (black surface), as a consequence of the electronic transition (tr. 1).

The geometry optimization of the first singlet excited state (S1) further supports its dissociative nature. The relaxed geometry displays a S–N bond length of 2.20 Å, about 0.25 Å longer with respect to the ground state (Fig. S29, ESI). Although S1 can be hardly populated directly by light absorption due to the extremely low value of the oscillator strength of the tr.1, Fig. 8A (which is also low for tr.2 and tr.3), it can be assumed that S1 is the arrival point of the de-excitation process from higher electronic excited states. Therefore, irradiation of $N(O)SO_3^-$ with light might lead to the formation of $NO^{\bullet}$ and $SO_3^{\bullet-}$, but this process seems to be favorable only for irradiation with UV light of higher energy (i.e. λirrad < 300 nm), in which the oscillator strengths have higher values (Fig. 8A). However, λ_{irrad} < 300 nm is out of the range used in this study.

Overall, our data support the view that the decomposition of $N(O)SO_3^-$ into $NO^{\bullet}$ and $SO_3^{\bullet-}$ (eqn (9)) could occur by both thermal and photochemical pathways. Nevertheless, because of the very low oscillator strengths predicted for $N(O)SO_3^-$ in the wavelength range of 300–900 nm (Fig. 8A), the thermal pathway is favored regarding the photochemical one. Moreover, based on the low energy

barrier predicted for the thermal homolysis of the S–N bond (~13 kcal mol^{-1}, Fig. 7), the dissociation of $N(O)SO_3^-$ (eqn (9)) should occur instantaneously at room temperature. Therefore, the irradiation of complex 1 with light leads to the photodissociation of $N(O)SO_3^-$ (Fig. 6), which then dissociates by the thermolysis of the S–N bond (Fig. 7), yielding $NO^{\bullet}$ and $SO_3^{\bullet-}$.

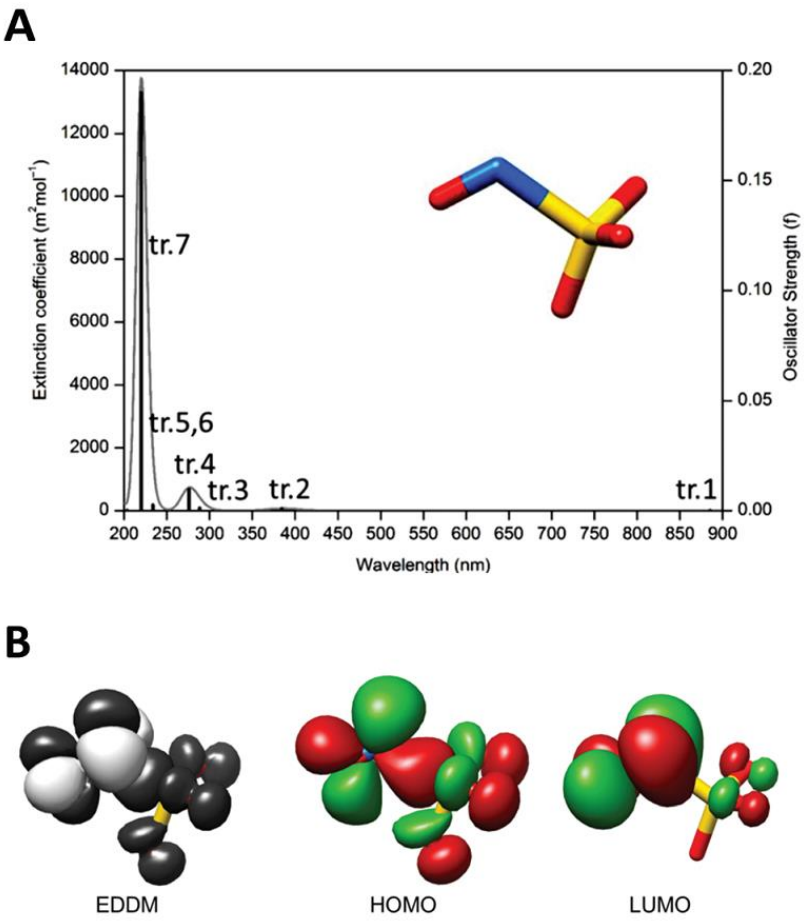

Fig. 8. (A) Theoretical electronic absorption spectrum (UV-Vis) of $N(O)SO_3^-$. Electronic transitions are represented as vertical bars with height equal to the oscillator strength (f) values. Inset: Structure of $N(O)SO_3^-$. (B) Electron-density difference maps (EDDM) (black indicates a decrease in electron density, white indicates an increase; isovalue = 0.001) and main component orbitals (HOMO and LUMO) of the 1st singlet–singlet transition (tr. 1) computed for N(O)SO3$^-$.

3. Conclusions

In summary, the stabilization of $N(O)SO_3^-$ provided by its coordination in complex **1** allowed us to better understand the chemical properties of this anion. Our study on the stability of **1** at neutral and acidic pH is in accordance with previous studies of nitrosylsulphito complexes. The electrophilic behavior described here for $N(O)SO_3^-$ in **1** is the first reported for nitrosylsulphito complexes, and we furthermore showed that the nucleophilic attack of OH^- on **1** produces the respective Ru(II) nitro complex. Therefore, these results provide a useful insight to understand the reaction pathways of $N(O)SO_3^-$ under biological conditions, where hydrolysis and attack by nucleophilic species are speculated. Also, the photochemical results presented here are the first described for the nitrosylsulphito complexes, and demonstrated the production of two important radicals, $NO^{\bullet}$ and

$SO_3^{\bullet-}$, when **1** was irradiated with light. In the context of applications, the main advantage of triggering the release of $NO^{\bullet}$ and $SO_3^{\bullet-}$ by light is the possibility of control of dosage and timing (i.e. on demand release). Hence, the results showed that complex **1** has significant potential as a photoactive source of the radical species $NO^{\bullet}$ and $SO_3^{\bullet-}$.

Based on the importance and applications of both nitric oxide and $SO_x^{\bullet-}$ radicals (eqn (1)–(4)), the studies performed here with complex **1** contribute to the development of other stable and water-soluble $[L_5M–N(O)SO_3]^n$ complexes tuned to release $NO^{\bullet}$ and $SO_3^{\bullet-}$ over an expanded range of wavelengths, mainly for biological purposes.

4. Experimental

4.1 Chemicals

Unless otherwise noted, reagents and solvents were purchased from Sigma-Aldrich, Merck or JT Baker at the highest quality available and were used without further purification. Milli-Q water (18.2 MΩ) was used throughout the experiments. Ruthenium(III) chloride hydrate (Strem Chemicals) was the synthetic precursor of all the ruthenium complexes. Sodium sulfite anhydrous (Na_2SO_3, Merck) was used for the synthesis of the nitrosylsulphito complexes. Unless otherwise noted, all solutions were deaerated with Ar (99.999%) for at least 30 min.

4.2 General

Electronic spectra (UV-Vis) were recorded on a Shimadzu UV3600 or in a Thermo Scientific Multiskan GO UV-Vis spectrophotometer, using a 1.00 cm quartz cell. Infrared spectra were recorded in a Shimadzu FTIR Spectrophotometer model IRAffinity-1 (for KBr pellets experiments), or in a Vertex 70v Bruker (for the experiments in solution). ^{1}H- and ^{15}N-NMR spectra were recorded on an Agilent 500 MHz NMR. Spectrometer (Model 500/54 Premium Shield). 3-(Trimethylsilyl)propionic-2,2,3,3-d4 (TMSP-d4) was used as an internal reference (δ = 0 ppm) for ^{1}H-NMR experiments, and a glass capillary filled with $^{15}NH_4Cl$ (δ = –354 ppm vs. chemical shift of CH_3NO_2, δ_{CH3NO2} = 0 ppm) was used as reference in the ^{15}N-NMR experiments. Electron paramagnetic resonance (EPR) spectra were recorded in a Bruker EMX Plus X-band spectrometer at room or liquid nitrogen temperature (77 K). Elemental analysis was performed in a PerkinElmer 2400 Series II CHNS/O Elemental Analyzer.

4.3 Syntheses

The synthetic precursor complexes [15,22,38] $[RuCl(NH_3)_5]Cl_3$, *trans*-$[RuCl(NH_3)_4(SO_2)]Cl$, *trans*-$[Ru(SO_4)(NH_3)_4(isn)]Cl$ (isn = isonicotinamide), *trans*-$[Ru(NH_3)_4(isn)(NO)](BF_4)_3$, and the aquo complex [31] *trans*-$[Ru(NH_3)_4(H_2O)(isn)](PF_6)_2$ were prepared and characterized as described elsewhere [15,22,31,38]. The ^{15}N-labeled *trans*-$[Ru(NH_3)_4(isn)(^{15}NO)](BF_4)_3$ was synthesized using $Na^{15}NO_2$ [28c].

4.3.1 Complex **1**, *trans*-$[Ru(NH_3)_4(isn)(N(O)SO_3)](PF_6)$

25 mg of complex **2** (4.3×10^{-5} mol) was added to 1.5 mL of argon degassed water at T = 25 °C, followed by the addition of 9 mg of sodium sulfite (Na_2SO_3, 7.1×10^{-5} mol) under vigorous stirring. After 1 min, 150 mg of NH_4PF_6 (9.2×10^{-4} mol) was added, resulting in the precipitation of crystals of the nitrosylsulphito complex after 30–60 min upon cooling on an ice-bath or a refrigerator. Yield

= 60–65%. Elemental Analysis ($C_6H_{18}F_6N_7O_5PRuS$) – Theoretical: C = 13.19%; H = 3.32%; N = 17.95%; S = 5.87%. Experimental: C = 13.60%; H = 3.39%; N = 17.79%; S = 5.69%.

4.3.2 *trans*-[$Ru(NH_3)_4(isn)(^{15}N(O)SO_3)](PF_6)$.
The ^{15}N-labeled complex *trans*-[$Ru(NH_3)_4(isn)(^{15}N(O)SO_3)](PF_6)$ (^{15}N-labeled complex **1**) was prepared following the same methodology described above, but using the ^{15}N-labeled precursor *trans*-[$Ru(NH_3)_4(isn)(^{15}NO)](BF_4)_3$ [28c].

4.4 X-ray data collection and structure determination

4.4.1 Complex **1**, *trans*-[$Ru(NH_3)_4(isn)(N(O)SO_3)](PF_6)$
A green crystal of dimensions 0.1 × 0.1 × 0.3 mm^3 was selected and mounted on an XtaLAB Mini Rigaku diffractometer. Data were collected at room temperature up to 52° in 2θ; final unit cell parameters were based on all reflections. Multi-scan absorption corrections were applied. Structure solution, refinement and hardware details are in the corresponding cif file. Listing of atomic coordinates and equivalent isotropic displacement parameters, full intramolecular bond distances and angles, hydrogen coordinates, and anisotropic thermal parameters are available from the authors and were deposited with the Cambridge Crystallographic Data Centre, reference number 1915847. Fig. 1 and Fig. S4 (ESI) were prepared using the software Mercury 3.9 [39]. Crystal data and structure refinement, listing of atomic coordinates and equivalent isotropic displacement parameters, and full intramolecular bond distances and angles are provided in Tables S1–S3 (ESI).

4.4.2 Complex **2**, *trans*-[$Ru(NH_3)_4(isn)(NO)](BF_4)_3$
The structure of complex **2** was solved by direct methods with SHELXS-97 [40]. The model was refined by full-matrix least squares on F^2 by means of SHELXL-97 [41]. All hydrogen atoms were stereochemically positioned and refined with the ridging model. Fig. 1 and S30 (ESI) were prepared using Mercury 3.9 [39]. Structure solution, refinement and hardware details are in the corresponding cif file. Listing of atomic coordinates and equivalent isotropic displacement parameters, full intramolecular bond distances and angles, hydrogen coordinates, and anisotropic thermal parameters of complex **2** are available from the authors and were deposited at the Cambridge Crystallographic Data Centre, reference number CCDC 1922883.

4.5 pKa of the $N(O)SO_3$ ligand in complex 1

An aqueous solution (20.0 mL) with pH 7.9 and I = 0.1 M (CF_3COONa) containing the complex *trans*-[$Ru(NH_3)_4(isn)(N(O)SO_3)]^+$ (C = 1.8 × 10^{-4} M) was titrated with small volumes (2.0–5.0 μL) of trifluoroacetic acid (HTFA) with a molarity of 0.01 to 1.0 M, and the progress was monitored by the decrease of the band at 363 nm by UV-Vis. The pKa was determined by spectrophotometry [42] through a graphical solution of eqn (10), where A = observed absorbance (absorbance of the mixture $A = A_I + A_M$), where A_M = absorbance of the molecular species, and A_I = absorbance of the ionized species.

$$pH = pKa + \log [(A-A_M)/(A_I-A)] \qquad (10)$$

pKa was also determined by the first and second derivative of the titration curve.

4.6 Stability of complex 1 in aqueous solutions

4.6.1 pH 7.4.

Stability assays of complex **1** were performed under phosphate buffer pH 7.4, C = 20 mM, I = 0.22 M CF_3COONa. The reaction course was followed by electronic spectroscopy (UV-Vis) at different temperatures; using the Arrhenius Equation and Eyring plots, the activation parameters, activation energy (E_a), enthalpy (ΔH), entropy (ΔS) of activation and Gibbs energy of activation (ΔG), were calculated. The reaction course was also monitored by ^{1}H-, and ^{15}N-NMR using the ^{15}N-labeled complex **1**.

4.6.2 1.0 M of trifluoroacetic acid (HTFA).

Complex **1** was solubilized in a solution of deuterated trifluoroacetic acid (DTFA, 1.0 M), and the product was characterized by ^{1}H-NMR. This result was compared to the ^{1}H-NMR spectrum of a solution of the nitrosyl complex **2** under the same conditions (1.0 M DTFA). FT-IR assays (in solution) were also performed for **1** in 1.0 M HTFA (trifluoroacetic acid), and in aqueous solution (control). The FT-IR spectrum of the nitrosyl complex (complex **2**) under the same conditions (1.0 M HTFA) was also recorded for comparisons.

4.7 Reaction of hydroxide ions (OH^-) with complexes 1 and 2

The reaction of complexes **1** and **2** with hydroxide ions (OH^-) was performed using the same methodology described for the reaction of a series of nitrosyl complexes with OH^- [24], which is briefly described below. The reaction progress was followed by electronic spectroscopy (UV-Vis), under pseudo-first order conditions ([OH−] ≫ [Ru]). Aqueous solutions of the Ru complexes (C_{Ru} = 1.0×10^{-4} M) and OH^- ranging from 0.01 M to 0.045 M, with ionic strength I = 1.0 M (NaCl), and in the temperature ranges T = 15 and 25 °C (for **1**) and 15 °C for **2**, were used. At least five experiments were performed for each concentration of OH^- used. This afforded at least 25 values for the observed rate constant (k_{obs}). Plots of k_{obs} versus [OH^-] were built for both complexes. In all cases, a linear distribution was observed. The slope was equal to the second-order rate constant. ^{15}N-NMR spectra were also recorded for the reaction of OH^- with the ^{15}N-labeled complexes **1** and **2** in order to characterize the products formed.

4.7.1 Photochemical experiments.

The UV light source was a Nd: YAG laser (Continuum, model Serulite-II) operating in the third harmonic (λ = 355 nm). The pulse energy was measured by using a power meter (Coherent, Lasermate-P) and was adjusted to ∼5 mJ per pulse; the pulse frequency was 10 pulses per s. Spectral changes during photolysis were measured by electronic spectroscopy (UV-Vis). The visible light source was a SD Laser 303, λ = 410 ± 5 nm, output power = 5 mW. For the photolysis followed by ^{1}H-NMR, solutions were placed in the NMR tube and irradiated in situ (with 410 nm light), or ex situ (with 355 nm light). For the EPR assays (detection of Ru(III)), solutions were irradiated in a cuvette at room temperature and then rapidly transferred to EPR tubes and frozen to N_2 liquid temperature (77 K) to record the spectra.

For the detection of the sulfite radical species ($SO_3^{\bullet-}$) by EPR spectroscopy, irradiation of **1** was performed in situ (quartz capilar), and the detection was accomplished using the spin trap 5,5-dimethyl-1-pyrroline N-oxide (DMPO). The EPR spectra were recorded at room temperature (T = 25 °C), and the spectrometer settings were as follows: modulation frequency, 100 kHz; modulation amplitude, 1.0 G; microwave power, 2 mW; microwave frequency, 9.79 GHz; field sweep, 100 G; receiver gain, 5×10^4; time constant, 20.48 ms; sweep time, 41.94 s; number of scans, 1. Computer simulations of the EPR spectra were performed using SimFonia software.

In the experiments using catalase (from bovine liver, 2000–5000 units per mg protein, Sigma) for the detection of nitric oxide ($NO^{\bullet}$), fresh stock solutions of catalase were prepared in phosphate buffer pH 7.4, diluted to reach the desired concentration (λ_{max} = 403 nm, $\varepsilon = 4.3\times10^5$ $M^{-1}cm^{-1}$) [29] and the photolysis was performed in a cuvette at T = 25 °C; the spectral changes were monitored by electronic spectroscopy (UV-Vis).
Experiments using oxymyoglobin (oxyMb) [28b,c] and carboxy PTIO [28a] for the detection of $NO^{\bullet}$ followed previously published procedures [28a,b,c]. Phosphate buffer solutions (pH 7.4) containing sodium sulfite (Na_2SO_3) and PTIO or oxyMB were photolyzed in a 1.00 path quartz cuvette; in the case of oxyMb, the reaction course was followed by UV-Vis spectroscopy, and in the case of PTIO, by EPR spectroscopy.
In all cases, the experimental details, such as concentration and temperature used, are described in the caption of the figures.

4.7.2 Laser flash photolysis (LFP).
LFP experiments were performed in a LFP-112 ns laser flash photolysis spectrometer (Luzchem Ottawa, Canada) using the third harmonic (355 nm) of a pulsed QSwitched Nd:YAG laser (Brilliant-B, LesUlis, France) attenuated to 15 mJ cm^{-2} as the excitation source with 8 ns of pulse duration. The signal from the photomultiplier detection system was captured by using a Tektronix TDS 2012 digitizer (Beaverton, OR, USA). The FFP-112 ns and the digitizer were connected to a personal computer via General Purpose Instrumentation Bus (GPIB) and serial interfaces controlling all the experimental parameters and providing suitable processing and data storage capabilities using a proprietary software package developed in a LabView environment and compiled as a stand-alone application (Luzchem, Ottawa, Canada). Each kinetic trace was averaged 16 times, and observed rate constants were determined by parameter fitting to exponential decay functions. All measurements were performed with aqueous phosphate buffer solutions pH 7.4 (20 mM, I = 0.22 M), thermostatted at 25.0 ± 0.5 °C, and purged with high-purity Argon for at least 30 min before the experiments. Samples were held under Argon in a round bottom flask, connected to a quartz flux cuvette by Tygon tubing, and pumped into the cuvette at a flow rate of about 0.5 mL min^{-1}.

4.7.3 Density functional theory (DFT).
All the calculations were performed by using the Gaussian 09 Revision C.01 (G09) program package [43], employing density functional theory (DFT) and time dependent (TD)-DFT methods [44]. Calculations were run using the Becke three-parameter hybrid functional [45], and the Lee–Yang–Parr gradient-corrected correlation functional (B3LYP) [46]. The solvent effect was included using the polarizable continuum model (PCM) with water as the solvent [47]. The SDD basis set [48] and effective core potential were used for the Ru atom. The 6-31G** basis set [49] was used for all the other atoms, while the photochemistry of $N(O)SO_3^-$ was treated at the 6-311++G** level. The complete reaction profile has been studied for the addition of OH^- to **1** (B3LYP/SDD/6-31G** level). Geometry optimizations were carried out without any symmetry constraints. The nature of the stationary points in the potential energy hypersurface was characterized either as minima or transition states by using harmonic vibrational frequency calculations. No imaginary frequencies were found for minima, thus indicating that we had located the minima on the potential-energy surfaces, while a single imaginary frequency was found for transition states. UV-Vis electronic absorption spectra of **1** and of $N(O)SO_3^-$ in the GS were simulated by using TD-DFT, computing a total of 80 and 16 singlet excited states, respectively. The electronic distribution and the localization

of the singlet excited states were visualized by using electron-density difference maps (EDDMs). GaussSum 2.2.550 was used to simulate the theoretical UV-Vis spectra and for the extraction of EDDMs [51]. Molecular-graphic images were produced by using the UCSF Chimera package from the Resource for Biocomputing, Visualization, and Informatics at the University of California, San Francisco [52]. For the thermal dissociation of $N(O)SO_3^-$, the reaction coordinate structures were calculated with the basis set qzvp, the functional B3LYP within the spin unrestricted formalism, and a water solvent (PCM). Transition state calculations were performed with the O–N–S–O dihedral frozen at 0 degrees from the eclipsed configuration.

5. Acknowledgements

The authors are grateful for the financial support by the Brazilian agencies FAPESP (12/23651-4, 17/01189-0) and CNPq (306491/2015-0). This study was financed in part by the Coordenação de Aperfeiçoamento de Pessoal de Nível Superior - Brasil (CAPES) - Finance Code 001. Dr. Gustavo Metzker is acknowledged for the critical review of this manuscript and Dr. Elena Amadio for help in the realization of the cover artwork.

References

[1] F. Bottomley, W. V. F. Brooks, D. E. Paez, P. S. White and M. Mukaida, J. Chem. Soc., Dalton Trans, 1983, 2465–2472.

[2] (a) U. Takahama and S. Hirota, J. Agric. Food Chem., 2012, 60, 1102–1112; (b) H. Vally, N. L. A. Misso and V. Madan, Clin. Exp. Allergy, 2009, 39, 1643–1651.

[3] a) P. B. Woolsey, J. Altern. Complement. Med., 2008, 14, 1159–1164; (b) C. Mottley, R. P. Mason, C. F. Chignell, K. Sivarajah and T. E. Eling, J. Biol. Chem., 1982, 257, 5050–5055; (c) K. Ranguelova, S. Chatterjee, M. Ehrenshaft, D. C. Ramirez, F. A. Summers, M. B. Kadiiska and R. P. Mason, J. Biol. Chem., 2010, 285, 24195–24205; (d) K. Ranguelova, A. B. Rice, A. Khajo, M. Triquigneaux, S. Garantziotis, R. S. Magliozzo and R. P. Mason, Free Radical Biol. Med., 2012, 52, 1264–1271; (e) K. Ranguelova, A. B. Rice, O. M. Lardinois, M. Triquigneaux, N. Steinckwich, L. J. Deterding, S. Garantziotis and R. P. Mason, Free Radical Biol. Med., 2013, 60,98–106; (f) M. Velayutham, C. F. Hemann, A. J. Cardounel and J. L. Zweier, Biochem. Biophys. Rep., 2016, 5,96–104; (g) W. T. Lee, Brain Dev., 2011, 33, 745–752.

[4] (a) H. J. Cohen and I. Fridovich, J. Biol. Chem., 1971, 246, 359–366; (b) J. L. Johnson and K. V. Rajagopalan, J. Biol. Chem., 1977, 252, 2017–2025; (c) K. Ranguelova and R. P. Mason, Free Radical Biol. Med., 2009, 47, 128–134.

[5] (a) E. Hayon, A. Treinin and J. Wilf, J. Am. Chem. Soc., 1972, 94,47–57; (b) P. Neta, R. E. Huie and A. B. Ross, J. Phys. Chem. Ref. Data, 1988, 17, 1027–1284.

[6] R. E. Huie and P. Neta, J. Phys. Chem., 1984, 88, 5665–5669.

[7] L. Eberson, Adv. Phys. Org. Chem., 1982, 18,79–185.

[8] Y. Guo, X. Lou, C. Fang, D. Xiao, Z. Wang and J. Liu, Environ. Sci. Technol., 2013, 47, 11174–11181.

[9] (a) Y. Deng and C. M. Ezyske, Water Res., 2011, 45, 6189–6194; (b) D. N. Zhou, H. Zhang and L. Chen, J. Chem. Technol. Biotechnol., 2015, 90, 775–779; (c) Y. Yang, J. Jiang, X. L. Lu, J. Ma and Y. Z. Liu, Environ. Sci. Technol., 2015, 49, 7330–7339; (d) L. S. Lian, B. Yao, S. D. Hou, J. Y. Fang, S. W. Yan and W. H. Song, Environ. Sci. Technol., 2017, 51, 2954–2962.

[10] M. Roginskaya, R. Mohseni, D. Ampadu-Boateng and Y. Razskazovskiy, Free Radical Res., 2016, 50, 756–766.

[11] (a) C. B. Bai, N. X. Wang, X. W. Lan, Y. J. Wang, Y. L. Xing, J. L. Wen, X. W. Gao and W. Zhang, Sci. Rep., 2016, 6, 20163; (b) Y. F. Guo, S. Mahmood, B. H. Xu, X. Q. Yao, H. Y. He and S. J. Zhang, J. Org. Chem., 2017, 82, 1591–1599.

[12] (a) S. N. Mendiara, E. Ghibaudi, L. J. Perissinotti and A. J. Colussi, J. Phys. Chem., 1992, 96, 8089–8091; (b) S. B. Oblath, S. S. Markowitz, T. Novakov and S. G. Chang, J. Phys. Chem., 1982, 86, 4853–4857.

[13] J. H. Swinehart, Coord. Chem. Rev., 1967, 2, 385–402.

[14] (a) W. Moser, R. A. Chalmers and A. G. Fogg, J. Inorg. Nucl. Chem., 1965, 27, 831–840; (b) A. G. Fogg, A. H. Norbury and W. Moser, J. Inorg. Nucl. Chem., 1966, 28, 2753–2755.

[15] E. Tfouni, M. Krieger, B. R. McGarvey and D. W. Franco, Coord. Chem. Rev., 2003, 236,57–69.

[16] (a) M. L. Souza, A. C. Roveda Jr., J. C. M. Pereira and D. W. Franco, Coord. Chem. Rev., 2016, 306, 615–627; (b) Y. Gao, A. Toubaei, X. Q. Kong and G. Wu, Chem. – Eur. J., 2015, 21, 17172–17177; (c) M. M. Cortese-Krott, A. R. Butler, J. D. Woollins and M. Feelisch, Dalton Trans., 2016, 45, 5908–5919; (d) M. A. Rhine, B. C. Sanders, A. K. Patra and T. C. Harrop, Inorg. Chem., 2015, 54, 9351–9366; (e) Y. Gao, B. Mossing and G. Wu, Dalton Trans., 2015, 44, 20338–20343; (f) J. C. M. Pereira, M. L. Souza and D. W. Franco, Eur. J. Inorg. Chem., 2015, 2015, 1005–1011; (g) L. L. Perissinotti, D. A. Estrin, G. Leitus and F. Doctorovich, J. Am. Chem. Soc., 2006, 128, 2512–2513; (h) L. L. Perissinotti, G. Leitus, L. Shimon, D. Estrin and F. Doctorovich, Inorg. Chem., 2008, 47, 4723–4733; (i) F. Roncaroli and J. A. Olabe, Inorg. Chem., 2005, 44, 4719–4727; (j) M. R. Filipovic, M. Eberhardt, V. Prokopovic, A. Mijuskovic, Z. Orescanin-Dusic, P. Reeh and I. Ivanovic-Burmazovic, J. Med. Chem., 2013, 56, 1499–1508; (k) S. L. Quiroga, A. E. Almaraz, V. T. Amorebieta, L. L. Perissinotti and J. A. Olabe, Chem. – Eur. J., 2011, 17, 4145–4156.

[17] T. Chivers and R. S. Laitinen, Chem. Soc. Rev., 2017, 46, 5182–5192.

[18] (a) W. Deng, H. L. Zhao, F. P. Pan, X. H. Feng, B. Jung, A. Abdel-Wahab, B. Batchelor and Y. Li, Environ. Sci. Technol., 2017, 51, 13372–13379; (b) A. Fraix and S. Sortino, Photochem. Photobiol. Sci., 2018, 17, 1709–1727; (c) R. Radi, Proc. Natl. Acad. Sci. U. S. A., 2018, 115, 5839–5848; (d) S. Sortino, Chem. Soc. Rev., 2010, 39, 2903–2913; (e) L. Chen, M. Tang, C. Chen, M. Chen, K. Luo, J. Xu, D. Zhou and F. Wu, Environ. Sci. Technol., 2017, 51, 12663–12671; (f) D. N. Zhou, L. Chen, J. J. Li and F. Wu, Chem. Eng. J., 2018, 346, 726–738.

[19] D. M. P. Mingos, Nitrosyl Complexes in Inorganic Chemistry, Biochemistry and Medicine I, Springer, Heidelberg, New York, Dordrecht, London, 2014.

[20] R. M. Carlos, D. R. Cardoso, E. E. Castellano, R. Z. Osti, A. J. Camargo, L. G. Macedo and D. W. Franco, J. Am. Chem. Soc., 2004, 126, 2546–2555.

[21] A. F. Holleman and E. Wiberg, Inorganic Chemistry, Academic Press, San Diego; De Gruyter, Berlin, New York, 2001.

[22] S. S. Borges, C. U. Davanzo, E. E. Castellano, J. Z-Schpector, S. C. Silva and D. W. Franco, Inorg. Chem., 1998, 37, 2670–2677.

[23] F. Doctorovich and F. Di Salvo, Acc. Chem. Res., 2007, 40, 985–993.

[24] F. Roncaroli, M. E. Ruggiero, D. W. Franco, G. L. Estiu and J. A. Olabe, Inorg. Chem., 2002, 41, 5760–5769.

[25] M. A. Il'yin, V. A. Emel'anov, A. V. Belyaev, A. N. Makhinya, S. V. Tkachev and N. I. Alferova, Russ. J. Inorg. Chem., 2008, 53, 1070–1076.

[26] F. Bottomley, Acc. Chem. Res., 1978, 11, 158–163.

[27] (a) C. A. Bignozzi, C. Chiorboli, Z. Murtaza, W. E. Jones and T. J. Meyer, Inorg. Chem., 1993, 32, 1036–1038; (b) R. G. Lima, M. G. Sauaia, D. Bonaventura, A. C. Tedesco, R. F. V. Lopez, L. M. Bendhack and R. S. da Silva, Inorg. Chim. Acta, 2005, 358, 2643–2650.

[28] (a) A. C. Roveda Jr., T. B. R. Papa, E. E. Castellano and D. W. Franco, Inorg. Chim. Acta, 2014, 409 part A, 147–155; (b) A. C. Merkle, A. B. McQuarters and N. Lehnert, Dalton Trans., 2012, 41, 8047–8059; (c) A. C. Roveda Jr., H. D. Aguiar, K. M. Miranda, C. C. Tadini and D. W. Franco, J. Mater. Chem. B, 2014, 2, 7232–7242.

[29] M. Hoshino, K. Ozawa, H. Seki and P. C. Ford, J. Am. Chem. Soc., 1993, 115, 9568–9575.

[30] G. R. Buettner, Free Radical Biol. Med., 1987, 3, 259–303.

[31] (a) C. C. Kuehn and H. Taube, J. Am. Chem. Soc., 1976, 98, 689–702; (b) S. S. Isied and H. Taube, Inorg. Chem., 1976, 15, 3070–3075.

[32] (a) M. R. Camilo, C. R. Cardoso, R. M. Carlos and A. B. P. Lever, Inorg. Chem., 2014, 53, 3694–3708; (b) P. C. Ford, Chem. Sci., 2016, 7, 2964–2986; (c) G. Malouf and P. C. Ford, J. Am. Chem. Soc., 1977, 99, 7213–7220.

[33] (a) R. J. Singh, N. Hogg, J. Joseph and B. Kalyanaraman, J. Biol. Chem., 1996, 271, 18596–18603; (b) M. Marazzi, A. Lopez-Delgado, M. A. Fernandez-Gonzalez, O. Castano, L. M. Frutos and M. Temprado, J. Phys. Chem. A, 2012, 116, 7039–7049; (c) R. J. Singh, N. Hogg, J. Joseph and B. Kalyanaraman, FEBS Lett., 1995, 360,47–51.

[34] M. Nava, M. A. Martin-Drumel, C. A. Lopez, K. N. Crabtree, C. C. Womack, T. L. Nguyen, S. Thorwirth, C. C. Cummins, J. F. Stanton and M. C. McCarthy, J. Am. Chem. Soc., 2016, 138, 11441–11444.

[35] (a) S. J. Blanksby and G. B. Ellison, Acc. Chem. Res., 2003, 36, 255–263; (b) E. R. Cohen, T. Cvitas, J. G. Frey, B. Holmström, K. Kuchitsu, R. Marquardt, I. Mills, F. Pavese, M. Quack, J. Stohner, H. L. Strauss, M. Takami and A. J. Thor, Quantities, Units and Symbols in Physical Chemistry, IUPAC Green Book, 3rd edn, IUPAC & RSC Publishing, Cambridge, 2007.

[36] J. W. Ochterski, Thermochemistry in Gaussian, (accessed November, 2018).

[37] M. D. Bartberger, J. D. Mannion, S. C. Powell, J. S. Stamler, K. N. Houk and E. J. Toone, J. Am. Chem. Soc., 2001, 123, 8868–8869.

[38] M. G. Gomes, C. U. Davanzo, S. C. Silva, L. G. F. Lopes, P. S. Santos and D. W. Franco, J. Chem. Soc., Dalton Trans, 1998, 601–607.

[39] C. F. Macrae, P. R. Edgington, P. McCabe, E. Pidcock, G. P. Shields, R. Taylor, M. Towler and J. van De Streek, J. Appl. Crystallogr., 2006, 39, 453–457.

[40] G. M. Sheldrick, SHELXS97 Program for Crystal Structure Refinement, University of Gottingen, Gottingen, Germany, 1997.

[41] G. M. Sheldrick, SHELXS97, Program for Crystal Structure Analysis, University of Gottingen, Gottingen, Germany, 1997.

[42] A. Albert and E. P. Serjeant, The Determination of Ionization Constants: A Laboratory Manual, Chapman and Hall, New York, 1984.

[43] M. J. Frisch, G. W. Trucks, H. B. Schlegel, G. E. Scuseria, M. A. Robb, J. R. Cheeseman, G. Scalmani, V. Barone, B. Mennucci, G. A. Petersson, H. Nakatsuji, M. Caricato, X. Li, H. P. Hratchian, A. F. Izmaylov, J. Bloino, G. Zheng, J. L. Sonnenberg, M. Hada, M. Ehara, K. Toyota, R. Fukuda, J. Hasegawa, M. Ishida, T. Nakajima, Y. Honda, O. Kitao, H. Nakai, T. Vreven, J. A. Montgomery Jr., J. E. Peralta, F. Ogliaro, M. Bearpark, J. J. Heyd, E. Brothers, K. N. Kudin, V. N. Staroverov, R. Kobayashi, J. Normand, K. Raghavachari, A. Rendell, J. C. Burant, S. S. Iyengar, J. Tomasi, M. Cossi, N. Rega, J. M. Millam, M. Klene, J. E. Knox, J. B. Cross, V. Bakken, C. Adamo, J. Jaramillo, R. Gomperts, R. E. Stratmann, O. Yazyev, A. J. Austin, R. Cammi, C. Pomelli, J. W. Ochterski, R. L. Martin, K. Morokuma, V. G. Zakrzewski, G. A. Voth, P. Salvador, J. J. Dannenberg, S. Dapprich, A. D. Daniels, Ö. Farkas, J. B. Foresman, J. V. Ortiz, J. Cioslowski and D. J. Fox, Gaussian 09, Gaussian, Inc., Wallingford CT, 2009.

[44] (a) M. E. Casida, C. Jamorski, K. C. Casida and D. R. Salahub, J. Chem. Phys., 1998, 108, 4439–4449; (b) R. E. Stratmann, G. E. Scuseria and M. J. Frisch, J. Chem. Phys., 1998, 109, 8218–8224.

[45] A. D. Becke, J. Chem. Phys., 1993, 98, 5648–5652.
[46] C. T. Lee, W. T. Yang and R. G. Parr, Phys. Rev. B: Condens. Matter Mater. Phys., 1988, 37, 785–789.
[47] (a) M. Cossi, G. Scalmani, N. Rega and V. Barone, J. Chem. Phys., 2002, 117,43–54; (b) S. Miertuš, E. Scrocco and J. Tomasi, Chem. Phys., 1981, 55, 117–129.
[48] P. Fuentealba, H. Preuss, H. Stoll and L. Vonszentpaly, Chem. Phys. Lett., 1982, 89, 418–422.
[49] A. D. Mclean and G. S. Chandler, J. Chem. Phys., 1980, 72, 5639–5648.
[50] N. M. O'Boyle, A. L. Tenderholt and K. M. Langner, J. Comput. Chem., 2008, 29, 839–845.
[51] (a) W. R. Browne, N. M. O'Boyle, J. J. McGarvey and J. G. Vos, Chem. Soc. Rev., 2005, 34, 641–663; (b) M. Head-Gordon, A. M. Grana, D. Maurice and C. A. White, J. Phys. Chem., 1995, 99, 14261–14270.
[52] E. F. Pettersen, T. D. Goddard, C. C. Huang, G. S. Couch, D. M. Greenblatt, E. C. Meng and T. E. Ferrin, J. Comput. Chem., 2004, 25, 1605–1612.